Chinese Chemical Letters 37 (2026) 111189

Contents lists available at ScienceDirect

Chinese Chemical Letters

journal homepage: www.elsevier.com/locate/cclet

A unique two-fold interpenetrated zeolite-like metal–organic framework with SOD topology for one-step C_2H_4 purification from ternary mixtures

Jianyun Li[a,1], Lifei Zou[b,1], Jianwei Cao[c], Zhaohui Shi[a], Zhiwei Liu[a], Lirong Zhang[a], Jiyang Li[a], Xin Liu[d,*], Yunling Liu[a,*]

[a] College of Chemistry, State Key Laboratory of Inorganic Synthesis and Preparative Chemistry, Jilin University, Changchun 130012, China
[b] College of Chemistry and Life Science, Inner Mongolia Key Laboratory of Photoelectric Functional Materials, Chifeng University, Chifeng 024000, China
[c] School of Chemistry and Chemical Engineering, Key Laboratory of Special Functional and Smart Polymer Materials of Ministry of Industry and Information Technology, Xi'an Key Laboratory of Functional Organic Porous Materials, Northwestern Polytechnical University, Xi'an 710072, China
[d] School of Chemistry, Dalian University of Technology, Dalian 116024, China

ARTICLE INFO

Article history:
Received 11 February 2025
Revised 31 March 2025
Accepted 9 April 2025
Available online 10 April 2025

Keywords:
Zeolite-like metal–organic frameworks (ZMOFs)
2-Fold interpenetrated
Design strategies
Ethylene purification
Polar sites

ABSTRACT

Zeolite-like metal–organic frameworks (ZMOFs) are a unique branch of MOFs, compared to MOFs, the design and synthesis of ZMOFs is challenging due to the peculiar T-O-T angle. Herein, the first ZMOF with unique two-fold interpenetrated SOD topology, $[(CH_3)_2NH_2][Zn(2,5\text{-}ABTC)_{0.5}(TAZ)]\cdot DMF\cdot H_2O$ (**JLU-MOF119**, 2,5-H_4ABTC = 2,2′,5,5′-azobenzene tetracarboxylic, TAZ = 1*H*-tetraazol, DMF = *N*,*N*-dimethylformamide), was successfully constructed by utilizing a novel 4 + 4 + 2 strategy. In such a structure, the 4-connected 2,5-H_4ABTC ligand serves as the 4-membered ring (4MR) of the structural building units, and the TAZ linker coordinates with the Zn^{2+} center to form a 6-membered ring (6MR), which assembles with the tetrahedral building units (TBU) to construct the SOD topology. Notably, the stretched and distorted 4MR, which gives rise to two distinct 6MR and a twisted framework, finally leads to the formation of a unique 2-fold interpenetrated SOD framework. The pore structure of **JLU-MOF119** is featured by the ultra-microporous pore and the polar surface of the SOD cages caused by uncoordinated N and O sites coming from 2,5-H_4ABTC and TAZ ligands, resulting in one-step C_2H_4 purification from $C_2H_2/CO_2/C_2H_4$ mixtures. The dynamic breakthrough and recycling experiments confirm that the C_2H_4 purity is high up to 99.2 %. The successful construction of **JLU-MOF119** in this work breaks the theory of forbidden interpenetration in ZMOFs, which will provide more possibilities for structural design and the construction of more complicated structures.

© 2026 Published by Elsevier B.V. on behalf of Chinese Chemical Society and Institute of Materia Medica, Chinese Academy of Medical Sciences.

Ethylene (C_2H_4) is an essential feedstock for the chemical industry, and its downstream chemicals account for the majority of petrochemical products. Presently, three main processes are used to prepare C_2H_4: Naphtha cracking, oxidation and dehydrogenation (ODH) of ethane, and coal-to-ethylene. Nevertheless, in response to increasingly severe environmental issues and cost-cutting, researchers have developed more production processes with lower energy consumption, fewer pollutant emissions, and higher ethylene recovery rates. The oxidative coupling of methane (OCM) for ethylene, which involves a simple and cost-effective process, is a highly promising technique for ethylene production [1]. In the OCM process, the C–H bond is activated by O_2 to generate radicals, which then undergo dehydrogenative coupling to form C_2H_4, while the extensive thermals released in the process may cause over oxidation of C_2H_4 to produce C_2H_2, CO_2, and other byproducts. For the sake of downstream products made from C_2H_4, removing C_2H_4 from other byproducts is critically important. Considering the cost and environmental impact, porous materials show great potential in separating C_2H_4 from light hydrocarbon mixtures. Since their slight difference in quadrupole moments (C_2H_2: 7.2×10^{-26} esu cm^2, CO_2: 4.3×10^{-26} esu cm^2, C_2H_4: 1.5×10^{-26} esu cm^2) and kinetic sizes (C_2H_2: 3.3 Å, CO_2: 3.3 Å, C_2H_4: 4.2 Å) (Table S1 in Supporting information), one-step purification of C_2H_4 from $C_2H_2/CO_2/C_2H_4$ ternary mixtures is extremely challenging. Therefore, an effective strategy to address this challenge is to design and synthesize a polar structure, wherein a negative electro-

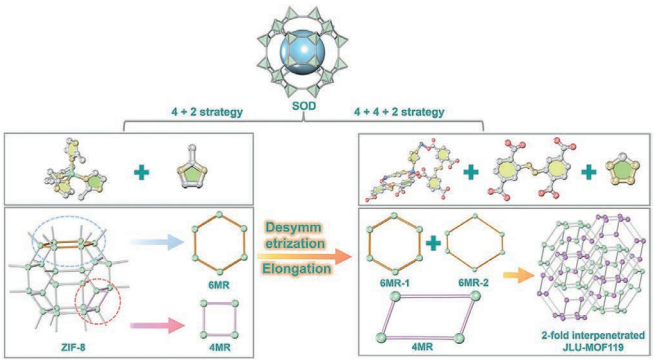
* Corresponding authors.
E-mail addresses: xliu@dlut.edu.cn (X. Liu), yunling@jlu.edu.cn (Y. Liu).
[1] These authors contributed equally to this work.

https://doi.org/10.1016/j.cclet.2025.111189
1001-8417/© 2026 Published by Elsevier B.V. on behalf of Chinese Chemical Society and Institute of Materia Medica, Chinese Academy of Medical Sciences.

static potential environment within the pores facilitates the enhancement of adsorption differentiation among gas molecules with distinct polarities. Metal–organic frameworks (MOFs) are a class of porous and inorganic-organic hybrid materials. Currently, the pore size designability and modifiability of MOFs have reached the range of sub-angstrom, thus providing great potential in separating molecules with subtle differences, such as C_2H_2/CO_2 [2–4], C_2H_6/C_2H_4 [5,6], and xylene isomers separation [7–9]. However, most of the reported MOFs have a poor selectivity for both C_2H_2/C_2H_4 and CO_2/C_2H_4 because of their similar physical properties, so it is still difficult to realize one-step purification C_2H_4 from $C_2H_2/CO_2/C_2H_4$ ternary mixtures [10–13]. In the view of pore structure, reducing the pore size of MOFs is one way to improve selectivity, proper apertures allow the framework to selectively capture small gases while excluding larger gases. Therefore, the design and synthesis of new and polar ultra-microporous MOFs is mandatory considering the kinetic sizes and quadrupole moments of C_2H_2, CO_2, and C_2H_4.

Zeolite-like metal–organic frameworks (ZMOFs) are a unique branch of MOFs, which exceed zeolites and other MOFs in gas storage and separation application [14–19]. Compared to traditional MOFs, the advantages of ZMOFs primarily lie in their cage-like cavities and ultra-microporous window sizes, which are beneficial for enhancing adsorption capacity and selective adsorption performance. Additionally, the anionic or cationic nature of some ZMOFs can be exploited to tailor the frameworks' affinity for certain gases, improving separation performance. Compared to other ZMOFs topologies, the sodalite (SOD) net is the most common occurrence, owing to its simple tiling of edge-transitive nets (1121). Specifically, the SOD cage is composed of six four-membered rings (4MR) and eight six-membered rings (6MR), while the sodalite network is a 3D structure formed by the interconnected SOD cages through their coplanar assembly. Through the unremitting efforts of researchers, how to construct the SOD topological ZMOFs has made substantial strides. For example, Eddaoudi's group used the Zr_6 cluster as a tetrahedral building unit (TBU) and judiciously selected the bent ditopic linker with steric hindrance to construct the Zr-sod-ZMOFs [20]. Subsequently, they utilized the centring structure-directing agents (cSDA) with appropriate geometry to prepare 21 types of ZMOFs with SOD topology, during which Fe-sod-ZMOFs-320 possessed the largest pore volume (3.21 cm^3/g) of sodalite compounds and exhibited the outstanding gas storage performance [21]. ZIF-8 with SOD topology can be regarded as a potential ideal material for gas separation due to its ultra-microporous pore size (3.4 Å) and high porosity (0.66 cm^3/g). However, ZIF-8 shows poor separation ability in slightly different gases (*e.g.*, C_2H_2, CO_2, and C_2H_4) owing to its nonpolar skeleton. To solve this problem, a feasible strategy is to construct an interpenetrated SOD structure that can fine-tune the pore size under sub-angstrom and increase the number of active sites per unit volume. However, rare examples of interpenetrated ZMOFs have been witnessed on account of the trait of zeolite type [22,23], and theoretically, the SOD net is not self-dual and forbidden self-interpenetration. Therefore, it remains a great challenge for the synthesis of interpenetrated SOD-based ZMOFs.

In this work, we first proposed a feasible 4 + 4 + 2 strategy to prepare a novel ZMOF (namely **JLU-MOF119**) with a unique two-fold interpenetrated SOD topology based on the 4 + 2 strategy for ZIF-8 synthesis (Scheme 1). Specifically speaking, based on the 4 + 2 strategy, besides the TBU served by the 4-connected metal node and a 2-connected linker (such as imidazole) to generate the 6MR, a coplanar 4-connected linker is properly chosen to replace some 2-connected linker and serves as the 4MR. In such 4 + 4 + 2 strategy, lengthening of the 4-connected ligand is crucial to construct interpenetrated structures. Given that, following our previous work of JLU-MOF52 (GIS) [24], a 2,5-H_4ABTC ligand with low



Scheme 1. Illustration of design strategy of 2-fold interpenetrated SOD topology in **JLU-MOF119**.

symmetry was utilized as the 4-c ligand. Such ligand may transform its configuration from tetrahedron (in JLU-MOF52) to parallelogram like 3,5-H_4ABTC in PCN-250 in appropriate conditions [25]. Meanwhile, to increase the number of polar sites, the imidazole in ZIF-8 is replaced by the TAZ ligand. As a result, the prepared **JLU-MOF119** possesses the SOD cage with abundant uncoordinated O and N sites, and the ultra-microporous pore size (4.1 Å and 3.3 Å). **JLU-MOF119** exhibits one-step purification C_2H_4 from ternary mixtures of $C_2H_2/CO_2/C_2H_4$, reaching 99.2 % purity of C_2H_4, as proved by the breakthrough and recycling experiments.

According to the reported ZMOFs, constructing the SOD ZMOFs involves several strategies: (1) 4 + 2 strategy, *i.e.*, 4-connected single-metal-ion nodes serve as TBU bridge by ditopic linker [26–30], (2) 4 + 4 strategy, *i.e.*, bridge the TBU with a tetrahedral tetratopic linker [31], (3) 4 + 6 strategy, *i.e.*, bridge the TBU with a hexacarboxylic linker [32], (4) face-directed strategy, *i.e.*, the linker serves as the face of the cage [33–36], (5) polyhedral assembly strategy, *i.e.*, the single-metal building blocks $\{In(COO)_4\}$ as the TBU to construct the SOD-type frameworks and the internal trinuclear clusters $\{In_3O\}$ form the tetrahedral cages (Fig. S1 in Supporting information) [37,38]. Here, based on the 4 + 2 strategy, a novel 4 + 4 + 2 strategy was proposed and successfully applied to prepare **JLU-MOF119** with unique 2-fold interpenetrated SOD net. Specifically, a portion of the imidazole ligands is replaced by 4-connected 2,5-H_4ABTC ligands, while the remaining imidazole ligands are substituted by TAZ ligands, thereby forming the 4 + 4 + 2 strategy. The employment of elongate 4MR results in two types of 6MR and distorted framework, eventually leading to the interpenetrated SOD structure.

The crystallography data reveals that **JLU-MOF119** crystallizes in a trigonal system with *R*-3 space group (Table S2 in Supporting information). In the skeleton, independent Zn^{2+} and 2,5-H_4ABTC adopt four coordination, and TAZ serves as a ditopic linker. Each Zn^{2+} is coordinated with two oxygen atoms from two individual 2,5-H_4ABTC ligands and two nitrogen atoms from different TAZ, respectively, to form the low-symmetry TBU, ZnN_2O_2 (Fig. 1a and Fig. S2a in Supporting information). Each independent 2,5-H_4ABTC ligand is linked to four Zn^{2+} and two TAZ, generating the 4MR (Fig. 1c and Fig. S2b in Supporting information). Moreover, each carboxyl group of 2,5-H_4ABTC contains an uncoordinated O atom and points into the SOD cage. Each individual TAZ linker is coordinated to two Zn^{2+} cations and then engenders the 6MR-1 (Fig. S2c in Supporting information), the adjacent TAZ linkers are interlaced, and the uncoordinated N atoms of TAZ point toward the center of the window. There are two kinds of 6MR in the framework, one is the regular 6MR-1, and the other is formed by two TAZ, four half of 2,5-H_4ABTC and six Zn^{2+} (Figs. 1c and d). In the 6MR-2, the TAZ serves as the shorter edge, and the half of 2,5-H_4ABTC serves as the longer edge, the length varies between TAZ and 2,5-H_4ABTC

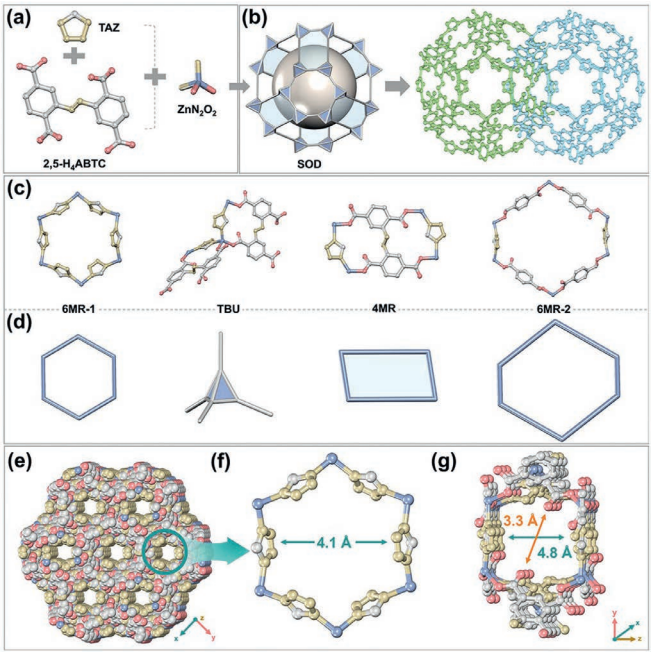


Fig. 1. Single crystal structure illustration of **JLU-MOF119**: (a) The Zn^{2+} node, TAZ, and 2,5-H_4ABTC linker. (b) Polyhedral view of one SOD cage and ball-and-stick view of 2-fold interpenetrated framework. (c) Ball-and-stick representations of the 6MR, TBU, and 4MR SBU. (d) Stick representations of the 6MR, TBU, and 4MR SBU. (e) The CPK view of **JLU-MOF119** framework. (f) The window size of 6MR. (g) Another type of window size after interpenetration. Color code: Zn, purple; C, gray; O, pink; N, brown.

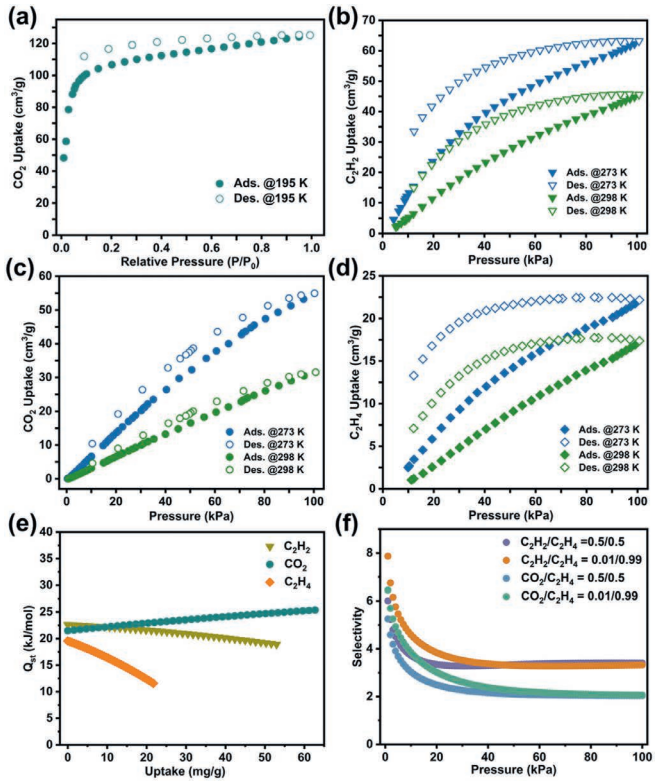


Fig. 2. **JLU-MOF119** adsorption/desorption isotherms: (a) 195 K CO_2, (b) C_2H_2, (c) CO_2 and (d) C_2H_4 at 273 K (blue) and 298 K (green). (e) Q_{st} for C_2H_2, CO_2, C_2H_4 of **JLU-MOF119**. (f) Selectivity for C_2H_2/C_2H_4 and CO_2/C_2H_4 mixtures predicted by IAST at 298 K and 1.0 bar.

resulting in the window of 6MR-2 is bigger than that of 6MR-1. From the topological perspective, the 4MR, 6MR-1, and 6MR-2 further extend to a 3D framework, which has the same underlying SOD topology as ZIF-8 (Fig. 1b), yet distinguishes it from the SOD net. In the **JLU-MOF119** framework, the 4MR with low symmetry and represents parallelogram, and other 4MR of ZMOFs with SOD net are mostly square. The twisted 4MR gives rise to the formation of 6MR with different sizes, which causes structural interpenetration and distortion of the framework (Fig. 1b). Thus, there are two types of apertures for **JLU-MOF119**, one is 6MR-1 forming a hexagonal aperture with size of 4.1 Å × 4.1 Å along the [001] direction and the other has a rectangular channel formed by interpenetrated 6MR-2 with size of 4.8 Å × 3.3 Å (Figs. 1e–g). It is noted that the pore structure of **JLU-MOF119** is distinct from ZIF-8 due to the interpenetrated framework, in which ZIF-8 only has one kind of hexagonal aperture and a significant smaller cage of SOD (11.6 Å *vs.* 18.6 Å), yet the cage of **JLU-MOF119** is reduced to 5.9 Å after the interpenetration of the framework (Fig. S3 in Supporting information).

Notably, **JLU-MOF119** possesses two kinds of ultra-microporous pores as well as better stability in various solvents and thermal stability before 210 °C (Figs. S4 and S5 in Supporting information), which endows it with potential adsorption and separation ability in light hydrocarbons mixtures. N_2 could not be adsorbed by **JLU-MOF119** for its ultra-microporous window size, thereby, CO_2 adsorption was used to evaluate the porosity of **JLU-MOF119** at 195 K. As shown in Fig. 2a, the uptake of **JLU-MOF119** is 125 cm^3/g at 195 K and 100 kPa. The Brunauer-Emmett-Teller (BET) and Langmuir surface areas of **JLU-MOF119** are 387 and 433 m^2/g, respectively. Light hydrocarbons are significant raw materials and industrial gases for the chemical industry, and the ultra-microporous window size of **JLU-MOF119** prompts us to hypothesize that it has the potential for the separation of light hydrocarbons. Therefore, **JLU-MOF119** was performed for single-component adsorption of N_2, CO_2, CH_4, C_2H_6, C_2H_4, C_2H_2, and C_3H_8 (Figs. 2b–d and Fig. S6 in Supporting information) at 273 and 298 K. Apparently, the gases of N_2, CH_4, C_2H_6, and C_3H_8 with bigger kinetic diameters are hardly adsorbed by **JLU-MOF119** at 273 and 298 K, the slight uptake is primarily attributed to the adsorption on the surface of **JLU-MOF119**. Simultaneously, the C_2H_2, CO_2, and C_2H_4 can be adsorbed by **JLU-MOF119**, these results are consistent with the ultra-microporous pore size, which means that **JLU-MOF119** exhibits a respectable size sieving effect. Moreover, the uptake of C_2H_4 (17.37 cm^3/g) is lower than that of C_2H_2 (45.61 cm^3/g) and CO_2 (31.54 cm^3/g) at 1.0 bar and 298 K, which uncovers the possibility of separating C_2H_2/C_2H_4 and CO_2/C_2H_4. Simultaneously, compared to ZIF-8, the advantage of the interpenetrated framework is more obvious in gas separation, which exhibits an increase in the uptake of gases with smaller size (*e.g.*, CO_2 and C_2H_2), while a significant decrease of bigger gas molecules (*e.g.*, C_2H_6, C_3H_8, and C_3H_6) [39–41]. Moreover, the adsorption capacity of **JLU-MOF119** for C_2H_2 remains stable after 12 cyclic tests, indicating that **JLU-MOF119** has excellent stability and C_2H_2 sorption capacity (Fig. S7 in Supporting information).

The isosteric heat of adsorption (Q_{st}) for C_2H_2, CO_2, and C_2H_4 was calculated by the Virial equation to estimate the affinity between gases and the skeleton. As shown in Fig. 2e, the Q_{st} of C_2H_2, CO_2, and C_2H_4 are 22.6, 21.5, and 19.55 kJ/mol respectively at zero-coverage, indicating a stronger affinity of C_2H_2 and CO_2 than C_2H_4. Additionally, all the values of Q_{st} are lower than the majority of MOFs, *e.g.*, FJI-H36 (36.1, 29.2, and 29.9 kJ/mol) [42], SNNU-98-Mn (60.2, 29.2, and 30.8 kJ/mol) [43], and ZNU-8 (33.1, 26.6, 25.7 kJ/mol) [4], which implies the low energy consumption for regeneration. The simulation of the adsorption isotherms and Q_{st} plots for the other gases are shown in Figs. S8–S11, Tables S3 and S4 (Supporting information).

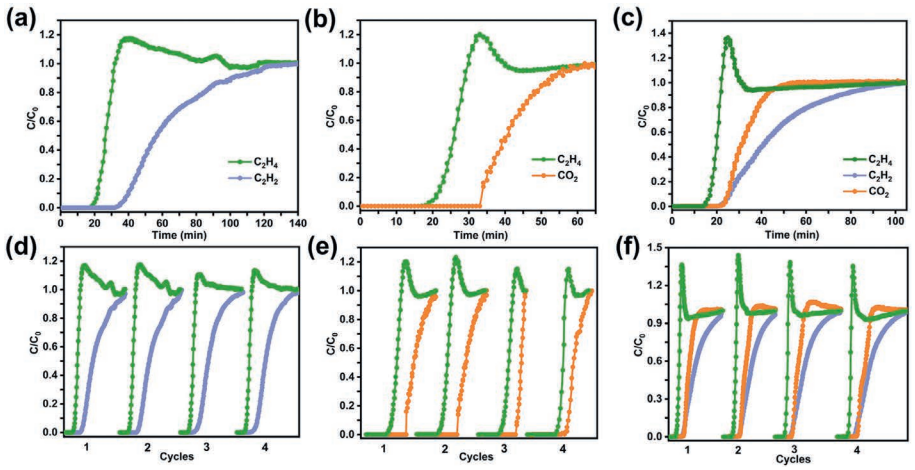


Fig. 3. Breakthrough experiments of (a) C_2H_2/C_2H_4 in equimolar at 2 mL/min (v/v = 1/1) and 298 K. (b) CO_2/C_2H_4 in equimolar at 2 mL/min (v/v = 1/1) and 298 K. (c) $C_2H_2/CO_2/C_2H_4$ in equimolar at 3 mL/min (v/v/v = 1/1/1) and 298 K. Cycles experiments for (d) C_2H_2/C_2H_4, (e) CO_2/C_2H_4 and (f) $C_2H_2/CO_2/C_2H_4$.

To assess the separation capacity, the adsorption selectivity was calculated by the ideal adsorption solution theory (IAST) of dual-site Langmuir-Freundlich model from single component adsorption isotherms. The selectivity for C_2H_2/C_2H_4 (50/50, 1/99, v/v) is 3.4 and 3.3 (Fig. 2f), higher than those reported MOFs of Fe-MOF-74 (2.08, 50/50) [44], BSF-1 (2.3, 50/50) [45], TJT-100 (1.8, 50/50) [46], JLU-MOF88 (3, 50/50) (Table S5 in Supporting information) [47]. The selectivity for CO_2/C_2H_4 (50/50, 1/99, v/v) is 2.03 and 2.05, higher than Zn-atz-oba (1.33, 50/50) [13], NKMOF-1-Ni (0.8, 50/50) [48]. Compared to reported MOFs in purification C_2H_4 from ternary mixtures of $C_2H_2/CO_2/C_2H_4$ (Fig. S12 and Table S6 in Supporting information), such as Zn-atz-oba (C_2H_2/C_2H_4, 1.33, CO_2/C_2H_4, 1.43) [13], Zn-fa-atz (C_2H_2/C_2H_4, 1.5, CO_2/C_2H_4, 1.4) [10], **JLU-MOF119** is an effective purification candidate for C_2H_4 from ternary mixtures of $C_2H_2/CO_2/C_2H_4$ by one step.

As is well known, compared to C_2H_4, C_2H_2, and CO_2 possess higher electron cloud densities. Therefore, a polar cage surface demonstrates a stronger affinity for C_2H_2 and CO_2. To thoroughly verify the practical application potential of **JLU-MOF119** for $C_2H_2/CO_2/C_2H_4$ separation, **JLU-MOF119** was executed the breakthrough experimental tests. The binary mixtures breakthrough experiments of C_2H_2/C_2H_4 and CO_2/C_2H_4 were performed in equimolar at 2 mL/min and 298 K (Figs. 3a and b). In Fig. 3a, the C_2H_4 is first flowed out at 17 min, while the C_2H_2 is eluted at 32 min. The experiment result is consistent with the static adsorption isotherm. Compared to separate C_2H_2/C_2H_4, the mixtures of CO_2 and C_2H_4 have closer quadrupole moments, which means it would be more obstacle to separate CO_2/C_2H_4. As indicated in Fig. 3b, the C_2H_4 is eluted at 17 min, and CO_2 is retained until eluted at 33 min, confirming **JLU-MOF119**'s exceptional CO_2/C_2H_4 separation performance. In the OCM process, C_2H_2, CO_2, and C_2H_4 are coexistent, thus the breakthrough experiment of $C_2H_2/CO_2/C_2H_4$ was executed at 3 mL/min and 298 K (Fig. 3c). As shown in Fig. 3c, the C_2H_4 is first flowed out at 14 min, while C_2H_2 and CO_2 are flowed out at 21 min and 22 min. And the purity of C_2H_4 reaches a high value of 99.2 % at the outlet before the C_2H_2 and CO_2 flow out further proving **JLU-MOF119** achieves one-step purification of C_2H_4 from $C_2H_2/CO_2/C_2H_4$ ternary mixtures. To better meet the practical application, cyclic tests on **JLU-MOF119** were performed to evaluate the regenerative capacity. As shown in Figs. 3d–f, the capacity of **JLU-MOF119** to separate C_2H_2/C_2H_4, CO_2/C_2H_4 and $C_2H_2/CO_2/C_2H_4$ remains virtually unchanged after 4 cycles. Moreover, the consistent C_2H_2 adsorption capacity after 12 cycles indicates that **JLU-MOF119** retains its selective C_2H_4 purification performance even after 12 breakthrough experiments (Fig. S7).

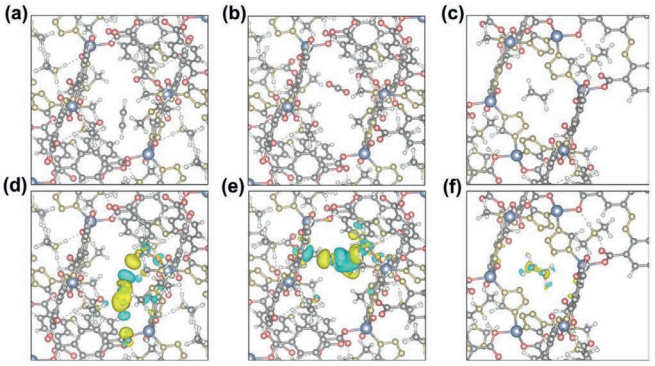


Fig. 4. The most plausible adsorption structures (a–c) and corresponding isosurface plots of charge density difference (d–f) of C_2H_2, CO_2 and C_2H_4 in **JLU- MOF119** viewed along *z* axis. In (a–f), the charge accumulation and charge depletion regions are in yellow and blue, respectively, and the isovalues are ±0.0003 a.u.

First-principles based calculations with empirical correction for dispersive interactions were performed to investigate the mechanisms that differentiate C_2H_2, CO_2, and C_2H_4 adsorption in **JLU-MOF119** (Figs. 4a–c) [49,50]. In the most plausible adsorption structure (Fig. S13 in Supporting information), C_2H_2 stays within the channel surrounded by Zn(II), TAZ, and dimethyl ammonia cations (DMA) (Fig. 4a), and the corresponding E_{ads} is 0.75 eV. C_2H_2 stays around the 6MR-2, it interacts mainly with the uncoordinated O of the 2,5-H_4ABTC at H(C_2H_2)–O(2,5-H_4ABTC) distance of 2.31 and 2.61 Å, respectively, and also interacts electrostatically with the TAZ right below it at C(C_2H_2)–N(DMA) and C(C_2H_2)–C(DMA) distances of 3.46 and 3.53 Å, respectively. C_2H_2 is also distorted slightly upon adsorption, the H–C–C and C–C–H angles are distorted from 180° when freestanding to 176.38° and 179.43°, respectively. These, together with the isosurface plot of charge density difference upon C_2H_2 adsorption suggest that dispersive interactions are formed to stabilize C_2H_2 (Fig. 4d).

Different from the case of C_2H_2, CO_2 would diffuse into the 6MR-2 opening to interact with the H of adjacent and nearly parallelly arranged TAZ ligands to gain additional stability (Fig. 4b), and the calculated E_{ads} is 0.31 eV. In this configuration, positively charged C(CO_2) interacts electrostatically with an H (2,5-H_4ABTC) and a carboxylic-O of uncoordination from adjacent 2,5-H_4ABTC ligands, and two O(CO_2) also interact with the 2 H of different TAZ ligands. The calculated O(2,5-H_4ABTC)–C(CO_2) and H(2,5-H_4ABTC)–C(CO_2) distances are 2.75 and 3.20 Å, respectively. The

calculated H(TAZ)−O(CO_2) distances are 2.89 and 3.29 Å, respectively. The O–C–O angle within CO_2 is also distorted from 180° to 177.89°. The isosurface plot of charge density difference upon CO_2 adsorption also suggests the dispersive nature of CO_2 adsorption with cooperative interactions with both negatively and positively charge centres of adjacent ligands that were previously proposed to account for enhanced CO_2 adsorption in microporous amorphous carbon (Fig. 4e).

The case of C_2H_4 is similar to that of C_2H_2 (Fig. 4c). Dispersive interactions are formed between C_2H_4 and TAZ ligands. The calculated H(C_2H_4)−N(TAZ) distances are 3.00, 3.05, 3.06, and 3.07 Å, respectively. C_2H_4 is also distorted slightly, the H–C–C angles are distorted from 121.69° when freestanding to 121.87° after adsorption. These together with the charge density difference upon C_2H_4 adsorption suggests that dispersive interactions account for C_2H_4 adsorption (Fig. 4f). The charge transfer accompanying C_2H_4 adsorption is less significant as compared with that of C_2H_2 and CO_2 (Figs. 4d and e), so C_2H_4 adsorption would be weaker. Accordingly, the calculated E_{ads} of C_2H_4 is 0.26 eV and C_2H_4 adsorption is the weakest among the three gases investigated.

In summary, a novel 4 + 4 + 2 strategy is designed to construct the first interpenetrated SOD-based ZMOF, **JLU-MOF119**. The 4 + 4 + 2 strategy is based on the 4 + 2 strategy of constructing ZIF-8, which is formed by using the 4-c ligand to replace a portion of 2-c ligand. Specifically, the former 4 refers to the TBU of ZnN_2O_2, which consists of TAZ and 2,5-H_4ABTC; the latter 4 refers to the 4-c ligand of 2,5-H_4ABTC; and the 2 refers to the 2-c ligand of TAZ. In such framework, the use of elongated and distorted ligand of 2,5-H_4ABTC results in the formation of two types of 6MR, and subsequently assemble into a distorted and interpenetrated SOD framework. **JLU-MOF119** possesses abundant uncoordinated N and O sites in the SOD cage and the ultra-microporous pore size, which represents a decent separation capacity of $C_2H_2/CO_2/C_2H_4$, and the C_2H_4 purity of 99.2 % is obtained by dynamic column breakthrough experiments. The simulations and calculations study gives more insight into the unique structure feature and the distinct affinity between gases of C_2H_2, CO_2, and C_2H_4 and the framework, accounting for the excellent selectivity of light hydrocarbons. This work pioneers a new and feasible strategy of SOD topology with interpenetrated structure, and explores new MOF materials applied in the field of multi-component light hydrocarbon separation, which also provides an effective pathway for designing structures with specialized functions.

Declaration of competing interest

The authors declare that they have no known competing financial interests or personal relationships that could have appeared to influence the work reported in this paper.

CRediT authorship contribution statement

Jianyun Li: Writing – original draft, Investigation, Conceptualization. **Lifei Zou:** Methodology, Investigation, Data curation. **Jianwei Cao:** Data curation. **Zhaohui Shi:** Data curation. **Zhiwei Liu:** Data curation. **Lirong Zhang:** Writing – review & editing, Supervision. **Jiyang Li:** Writing – review & editing. **Xin Liu:** Data curation. **Yunling Liu:** Writing – review & editing, Funding acquisition, Conceptualization.

Acknowledgments

This work was supported by the National Natural Science Foundation of China (Nos. 22171100 and U23A20360) and the '111 Center' (No. B17020). X. Liu was supported by National Natural Science Foundation of China (Nos. 21771029, 11811530631, and 21573034). The supercomputer time was provided by High Performance Computing Center at Dalian University of Technology. L. Zou was supported by National Natural Science Foundation of China (No. 22361001).

Supplementary materials

Supplementary material associated with this article can be found, in the online version, at doi:10.1016/j.cclet.2025.111189.

References

[1] J. Liu, J. Yue, M. Lv, et al., Carbon Res. Conv. 5 (2022) 1–14.
[2] J. Wang, Y. Zhang, Y. Su, et al., Nat. Commun. 13 (2022) 200.
[3] L. Zhang, T. Xiao, X. Zeng, et al., J. Am. Chem. Soc. 146 (2024) 7341–7351.
[4] Y. Zhang, W. Sun, B. Luan, et al., Angew. Chem. Int. Ed. 62 (2023) e202309925.
[5] G. Wang, R. Krishna, Y. Li, et al., Angew. Chem. Int. Ed. 61 (2022) e202213015.
[6] L. Li, R. Lin, R. Krishna, et al., Science 362 (2018) 443–446.
[7] J. Zhou, T. Ke, Y. Song, et al., J. Am. Chem. Soc. 144 (2022) 21417–21424.
[8] X. Cui, Z. Niu, C. Shan, et al., Nat. Commun. 11 (2020) 5456.
[9] X. Li, J. Wang, N. Bai, et al., Nat. Commun. 11 (2020) 4280.
[10] R. Yang, Y. Wang, J. Cao, et al., Nat. Commun. 15 (2024) 804.
[11] Y. Jiang, Y. Hu, B. Luan, et al., Nat. Commun. 14 (2023) 401.
[12] Q. Dong, Y. Huang, K. Hyeon-Deuk, et al., Adv. Fun. Mater. 32 (2022) 2203745.
[13] J. Cao, S. Mukherjee, T. Pham, et al., Nat. Commun. 12 (2021) 6507.
[14] M. Eddaoudi, D. Sava, J. Eubank, et al., Chem. Soc. Rev. 44 (2015) 228–249.
[15] Y. Tan, F. Wang, J. Zhang, Chem. Soc. Rev. 47 (2018) 2130–2144.
[16] A. Phan, C. Doonan, F. Uribe-Romo, et al., Acc. Chem. Res. 43 (2010) 58–67.
[17] F. Yi, H. Yang, X. Zhao, et al., Angew. Chem. Int. Ed. 58 (2019) 2889–2892.
[18] J. Li, D. Sava, V. Guillerm, et al., Chem 10 (2024) 567–577.
[19] K. Park, Z. Ni, A. Cote, et al., Proc. Natl. Acad. Sci. U. S. A. 103 (2006) 10186–10191.
[20] N. Alsadun, G. Mouchaham, V. Guillerm, et al., J. Am. Chem. Soc. 142 (2020) 20547–20553.
[21] M. Barsukova, A. Sapianik, V. Guillerm, et al., Nat. Synth. 3 (2024) 33–46.
[22] W. Xie, W. He, S. Li, et al., Chem. Eur. J. 22 (2016) 17298–17304.
[23] Y. Liu, M. Grzywa, M. Weil, et al., J. Solid State Chem. 183 (2010) 208–217.
[24] L. Zou, X. Sun, J. Yuan, et al., Inorg. Chem. 57 (2018) 10679–10684.
[25] D. Feng, K. Wang, Z. Wei, et al., Nat. Commun. 5 (2014) 5723.
[26] R. Banerjee, A. Phan, B. Wang, et al., Science 319 (2008) 939–943.
[27] X. Huang, Y. Lin, J. Zhang, et al., Angew. Chem. Int. Ed. 45 (2006) 1557–1559.
[28] Y. Liu, V. Kravtsov, R. Larsen, et al., Chem. Commun. 14 (2006) 1488–1490.
[29] B. Abrahams, M. Haywood, R. Robson, et al., Angew. Chem. Int. Ed. 42 (2003) 1112–1115.
[30] L. Tabares, J. Navarro, J. Salas, J. Am. Chem. Soc. 123 (2001) 383–387.
[31] L. Sun, H. Xing, Z. Liang, et al., Chem. Commun. 49 (2013) 11155–11157.
[32] W. Du, Z. Zhu, Y. Bai, et al., Chem. Commun. 54 (2018) 5972–5975.
[33] M. Dinca, W. Han, Y. Liu, et al., Angew. Chem. Int. Ed. 46 (2007) 1419–1422.
[34] Y. Tan, Y. He, J. Zhang, Chem. Commun. 47 (2011) 10647–10649.
[35] T. Mcdonald, D. D'Alessandro, R. Krishna, et al., Chem. Sci. 2 (2011) 2022–2028.
[36] M. Feng, X. Zhou, X. Wang, et al., ACS Appl. Mater. Interfaces 15 (2023) 11837–11844.
[37] S. Zheng, J. Bu, Y. Li, et al., J. Am. Chem. Soc. 132 (2010) 17062–17064.
[38] S. Zheng, T. Wu, F. Zuo, et al., J. Am. Chem. Soc. 134 (2012) 1934–1937.
[39] S. Xiang, W. Zhou, J. Gallegos, et al., J. Am. Chem. Soc. 131 (2009) 12415–12419.
[40] J. McEwen, J. Hayman, A. Yazaydin, Chem. Phys. 412 (2013) 72–76.
[41] L. Lyu, H. Wu, L. Li, et al., Chem. Ing. Tech. 94 (2022) 119–127.
[42] J. Tian, Q. Chen, F. Jiang, et al., Angew. Chem. Int. Ed. 62 (2023) e202215253.
[43] J. Wang, S. Fan, H. Li, et al., Angew. Chem. Int. Ed. 62 (2023) e202217839.
[44] E. Bloch, W. Queen, R. Krishna, et al., Science 335 (2012) 1606–1610.
[45] Y. Zhang, L. Yang, L. Wang, et al., Angew. Chem. Int. Ed. 131 (2019) 8229–8234.
[46] H. Hao, Y. Zhao, D. Chen, et al., Angew. Chem. Int. Ed. 130 (2018) 16299–16303.
[47] T. Xu, P. Zhang, F. Cui, et al., Adv. Mater. 35 (2023) 2204553.
[48] Y. Peng, T. Pham, P. Li, et al., Angew. Chem. Int. Ed. 57 (2018) 10971–10975.
[49] G. Kresse, J. Furthmuller, Phys. Rev. B 54 (1996) 11169–11186.
[50] E. Johnson, A. Becke, J. Chem. Phys. 124 (2006) 174104.